Journal of Physics: Condensed Matter

The analysis of charge transport mechanism in mixed ionic electronic conductor composite of Sr_2TiCoO_6 double perovskite with yttria stabilized zirconia

IOP Publishing Journal of Physics: Condensed Matter
J. Phys.: Condens. Matter **33** (2021) 315703 (12pp) https://doi.org/10.1088/1361-648X/ac0283

The analysis of charge transport mechanism in mixed ionic electronic conductor composite of Sr_2TiCoO_6 double perovskite with yttria stabilized zirconia

Sudha Saini[1,2], Kantesh Balani[2] and Tanmoy Maiti[1,*]

[1] Plasmonic and Perovskites Laboratory, Department of Materials Science and Engineering, Indian Institute of Technology Kanpur, UP 208016, India
[2] Biomaterials Laboratory, Department of Materials Science and Engineering, Indian Institute of Technology Kanpur, UP 208016, India

E-mail: tmaiti@iitk.ac.in

Received 21 December 2020, revised 3 May 2021
Accepted for publication 18 May 2021
Published 16 June 2021

Abstract

In this investigation, the ionic conduction mechanism in mixed ionic electronic conductors composites of Sr_2TiCoO_6/YSZ has been studied with the help of universal dynamic response. 3 mol% and 8 mol% yttria stabilized ZrO_2 have been mixed with Sr_2TiCoO_6 (STC) double perovskite in 1:1 ratio to prepare STC/3YSZ and STC/8YSZ composites via solid-state reaction route. AC Impedance spectroscopy has been carried out to examine the charge transport mechanism, which has been modeled using the microstructural networks of resistors and capacitors. Grain boundaries are more resistive and capacitive compared to the bulk. Modulus spectroscopy analysis demonstrates the non-Debye character of conductivity relaxation with frequency. Complex frequency-dependent AC conductivity is found to obey Almond West power law and reveals that ion migration occurs through the correlated hopping mechanism. Further, the DC conductivity and relaxation time have been found to follow the Barton Nakajima and Namikawa relation, which is correlated with AC to DC conduction. The time-temperature superposition principle has been used to explain the conductivity scaling in the intermediate frequency range. At low temperatures, the ions are localized in the asymmetric potential well, while at high temperatures, hopping behavior starts dominating. Further Kramers–Kronig transformation connects the dielectric strength with conductivity relaxation and verifies the impedance data.

Keywords: impedance spectroscopy, dielectric permittivity, mixed ionic electronic conductors, Almond West power law, SOFC

Supplementary material for this article is available online

(Some figures may appear in colour only in the online journal)

1. Introduction

Mixed ionic electronic conductor (MIEC) plays the vital role in the application of energy conversion and storage devices like fuel cells, batteries, oxygen permeable membranes, and memristive systems [1–6]. MIEC materials known for demonstrating both ionic as well as electronic conductivity are indispensable for electrochemical devices [7, 8], which contain three major components, such as anode, cathode, and oxygen ion-conducting electrolyte [9]. In general, MIEC also

* Author to whom any correspondence should be addressed.

possesses excellent mechanical durability and electrochemical functionality [10]. MIECs such as (Y, La, Nb, Fe, Mo, Ni, Mn) doped $SrTiO_3$ perovskites [11–15], $SrTiO_3$/YSZ [16, 17], and $SrTiO_3$/GDC [18, 19] composites have been reported in the literature for the application as electrode materials in SOFC. Yttria stabilized zirconia (YSZ) is the most commonly used electrolyte ionic conductor. Yttria doping in ZrO_2 gives rise to the oxygen vacancies to maintain the charge balance since a negatively charged Y^{+3} dopant occupies the place of Zr^{+4} lattice site [20]. These oxygen vacancies are further migrated through the electrolyte and affect the conversion efficiency of the fuel cell [21].

Among the various MIEC materials, donor or acceptor doped $SrTiO_3$ perovskites have demonstrated great potential as electrode material for electrochemical devices. These ceramics exhibit good electrical conductivity and similar thermal expansion coefficient like YSZ electrolyte [22]. However, these perovskites have some shortcomings, such as low catalytic activity, insufficient ionic conductivity, etc [16, 23]. Recently, the composites of perovskite and YSZ have gained lot of attention due to their long-term stability, MIEC, and reduced carbon deposition [24–27]. He *et al* have reported composites of YSZ with $Sr_{0.88}Y_{0.08}TiO_{3-\delta}$ (YST) as potential anode material for SOFC [26] demonstrating good stability in oxidizing and reducing atmosphere at high temperatures (1500 °C). However, they have found it difficult to increase the overall conductivity of YST/YSZ composites as any attempt in enhancing the electronic conductivity has led to the inferior ionic conductivity resulting in the conductivity of the composites as insufficient for attaining excellent performance of SOFC. Bochentyn *et al* [25] have investigated the MIEC composites of $SrTi_{0.98}Nb_{0.02}O_{3-\delta}$ (STN) with YSZ and ceria for the application as anode in SOFC. Because the processing of STN requires the synthesis under reducing atmosphere at high temperature, mechanical stress is generated within the STN based composite systems leading to low mechanical resistance [25]. Huang *et al* have studied the composite of YSZ with $La_{0.8}Sr_{0.2}MnO_3$ (LSM) for the application as the cathode for SOFC [27] and they have found that microstructural features such as grain boundaries play a crucial role in tuning the overall conductivity via oxygen vacancy, structural disorder, and precipitate formation. However the transport mechanism of these perovskite/YZS MIEC composites are yet to be understood. In the present work, attempt has been made to provide a unified model on the transport properties of MIEC composites. Recently, we have reported Sr_2TiCoO_6 (STC) double perovskite synthesized in air, demonstrating good electrical conductivity ~27 S cm^{-1} at 700 °C [28]. In the present work, the composite of STC and YSZ has been evaluated as MIEC and disordered dielectric solid since this system contains the random dispersal of conducting (STC) and insulating (YSZ) phases. To the best of our knowledge, this is the first report on transport properties of STC/YSZ MIEC composites. In the literature, disordered dielectric materials [29] have been observed to follow the universal dielectric response (UDR), proposed by Jonscher [30–33]. The anomalous dispersion power law of frequency-dependent dielectric permittivity and ac conductivity are the typical characteristics of disordered solids, composites, etc, found in their electrical properties. Almond *et al* have elucidated the detailed analysis of these ion-conducting universalities by using the array of microstructural networks [34–38]. These microstructural systems are generally modeled based on electrochemical impedance spectroscopy (EIS) data by using the chain of resistors and capacitors, which are associated with the grain and grain boundary of the material [34].

In the current investigation, we have synthesized STC/YSZ composites by solid-state reaction method and have investigated their microstructural and electrical properties using x-ray diffraction (XRD), field emission scanning electron microscopy (FESEM), and EIS. The conductivity isotherm is analyzed using Almond West (AW) power law, in correlation with the other physical models such as UDR, time-temperature superposition principle (the time-temperature superposition principle (TTSP)), Barton Nakajima and Namikawa (BNN) relation, and Kramers Kronig relation [40], which has provided the insights into the charge transport mechanism of this complex system. Furthermore, scaling analysis of the ac conductivity spectra has been carried out using TTSP [39].

2. Experimental procedure

Dense STC/YSZ composite samples of Sr_2TiCoO_6 with 3 mol% and 8 mol% yttria doped ZrO_2 labeled as 3YSZ and 8YSZ, respectively, are synthesized by using solid-state reaction route. First, Sr_2TiCoO_6 double perovskite has synthesized using the starting materials such as $SrCO_3$ (>99.9% purity, Sigma Aldrich), Co_3O_4 (>99.7%, Alfa Assar), and TiO_2 (>99.5% purity, Sigma Aldrich). Precursors are mixed adequately with ethanol for 24 h by using ball milling. The mixed powder has dried for overnight in an oven at 80 °C. Then, the powder is calcined at 1000 °C for 10 h. XRD has been performed to confirm the phase purity of the calcined STC powder. For the fabrication of STC/YSZ composite, the calcined powder Sr_2TiCoO_6 (STC), 3YSZ (>99.9%, 50 nm particle size, Nabond nano-technologies, Shenzhen, China) and 8YSZ (>99.9% Inframat® Advanced materials™ Manchester, USA) powders have been used. To synthesize the STC/3YSZ and STC/8YSZ composites, STC powder has been mixed with 3YSZ and 8YSZ powder, respectively, in weight % ratio of 1:1 for each composition. The mixed powder is milled in the planetary micro ball mill (Fritsch®, Pulverisette seven premium Line, Rhineland-Palatinate, Germany) at 600 rpm for 120 min, and ethanol is used as milling media. The milled powder is mixed with 2 wt.% polyvinyl alcohol and subsequently pressed into pellets of these composites. Sintering of STC/YSZ pellets is carried out at 1200 °C for 12 h. The phase purity of the composite materials has examined using the XRD profiles over 2θ (20–80°) range using the PANalytical X'Pert diffractometer. The micrograph of fractured STC/YSZ composites has been obtained via FESEM (FESEM, FEI-Nova NanoSEM 450, Germany) in backscattered electron mode. AC impedance spectroscopy measurement has been carried out via impedance analyzer (Solartron 1260 A, UK) with 1286 Solartron electrochemical interface between 250–650 °C temperature across

frequency range 10 MHz–0.1 Hz with an applied 500 mV AC amplitude in 5% H_2 and 95% N_2 atmosphere. The impedance measurement is carried out in a vertical furnace where the sample is mounted between the spring-loaded alumina plates, and platinum electrodes are used as the current collector for data acquisition. The EIS data is measured with a Δ (temperature difference) = 50 °C during the cooling cycle after stabilizing the temperature at each step. Before doing the measurement, the sample has coated with the platinum paste (Siltech Corporation, Bengaluru, India) on both surfaces and is baked at 900 °C for 1 h. Impedance measurement data has analyzed using the equivalent circuit fitting software (Zview, Scribner Associates Inc.USA) [41].

The response of the electrochemical cell has been represented in the complex Z^* plot. This complex impedance spectroscopic data can be formulated into the modulus, admittance, conductivity, and dielectric constant, which are defined by the following equations [42, 43]

$$Z^* = Z' + jZ'' \tag{1}$$

$$M^* = (\varepsilon^*)^{-1} = j\omega C_o Z^* = M' + jM'' \tag{2}$$

$$Y^* = \sigma^* = \frac{1}{Z^*} = j\omega\varepsilon^* \tag{3}$$

$$\sigma^* = \sigma' + j\sigma'', \tag{4}$$

where Z' and Z'' are real and imaginary part of impedance, M^* is the complex electrical modulus, M' and M'' are real and imaginary part of electric modulus, ε^* is dielectric constant, ω is the angular frequency, C_0 is vacuum capacitance, Y^* is complex admittance σ^* is the complex conductivity, σ' and σ'' are real and imaginary conductivity.

3. Result and discussion

The phase purity of STC/YSZ composite has been examined by XRD, illustrated in figure 1. XRD profiles of STC/3YSZ composite confirm the presence of both phases, i.e., STC as well as 3YSZ. However, a small amount of monoclinic ZrO_2 phase, which was initially present in the 3YSZ powder, has also been detected beside the tetragonal YSZ phase, as shown in figure 1(a). On the other hand, no such evidence of the minute monoclinic ZrO_2 has been detected in the XRD of STC/8YSZ composite, which shows only the presence of cubic STC double perovskites and 8YSZ, as shown in figure 1(b). The XRD peaks correspond to STC are found to be shifted toward the lower angle in both STC/3YSZ as well as STC/8YSZ composites, implying the increase in lattice constant of STC in these polycrystalline composites. The theoretical density of the composite is calculated using mixing law, which is defined by the following equation

$$\rho_t = v_1\rho_1 + v_2\rho_2, \tag{5}$$

where v_1 and v_2 are the volume fraction of STC and YSZ compounds, ρ_1, ρ_2 are the theoretical density of STC and YSZ, respectively. The Archimedes principle has been used to experimentally measure the density of these composites. The theoretically calculated density for STC/YSZ composites has been estimated as 5.675 g cm^{-3}. From the experimentally measured Archimedes density for both the composites, the calculated relative density of STC/3YSZ and STC/8YSZ samples are found to be ∼91% and ∼96%, respectively. Figures 1(c) and (d) show the microstructure of STC/YSZ composite, which is examined by the FESEM. Both the samples appeared to be adequately sintered. Although composite samples are appeared to be quite dense, ∼9% and ∼4% porosity is observed in STC/3YSZ and STC/8YSZ systems, respectively. The apparent porosity is beneficial for the SOFC system because it provides a path to flow the gas species. However, STC and YSZ are well bonded to each other and form a continuous network that provides the unremitting way for ions.

3.1. Electrical properties

The electrical properties of STC/YSZ composites have been measured using the EIS in the temperature range from 250 °C to 650 °C in 5% H_2 + 95% N_2 atmosphere. Figures 2 and S1 (https://stacks.iop.org/JPCM/33/315703/mmedia) illustrates the Nyquist plot of STC/8YSZ and STC/3YSZ, respectively. The figures indicate the high, intermediate, and low frequency semicircles, in which high frequency semicircle describes the bulk (grain) resistance, while intermediate and low frequency depressed arcs present the total resistance of grain boundary and electrode, respectively. The grain boundary capacitance ($\sim 10^{-10}$, F) has been found to be higher than the grain capacitance ($\sim 10^{-11}$, F), for both STC/8YSZ and STC/3YSZ composites. The shape of the semicircle is changed with the increasing temperature. A small arc is appeared at high frequency while low and intermediate frequency arc is seemed to be overlapped. The resistivity of the STC/8YSZ and STC/3YSZ composites for grain and grain boundary is decreased with increasing temperature, suggesting the increment in ionic conductivity. The overlapped low and intermediate frequency semicircle arc is found to be more significant than the high frequency semicircle, owing to the higher order of grain boundary polarization resistance against the intragrain polarization.

To determine the conductivity of the grain and grain boundary of composite samples, further, the impedance data have fitted with the circuit L, (R_g–Q_g), (R_{gb}–Q_{gb}), and (R_E–Q_E). Where L is the inductance, R_g, R_{gb}, and R_E are the resistance due to grain, grain boundary, and electrode. Q_g, $Q_{gb,}$ and Q_E are the constant phase elements of the grain, grain boundary, and electrode, respectively. The grain polarization resistance (R_g) and grain boundary polarization resistance (R_{gb}) values are estimated from the RC circuit fitting of the Nyquist plot. The calculated grain and grain boundary conductivity for STC/8YSZ at 650 °C temperature are found to be 1.58 mS cm^{-1} and 0.06 mS cm^{-1}, respectively. STC/3YSZ composite shows better conductivity at 650 °C, estimated as 2.55 mS cm^{-1} and 0.6 mS cm^{-1} for grain and grain boundary, respectively.

Further, the activation energy for grain and grain boundary is calculated from the gradient obtained in the linearly fitted

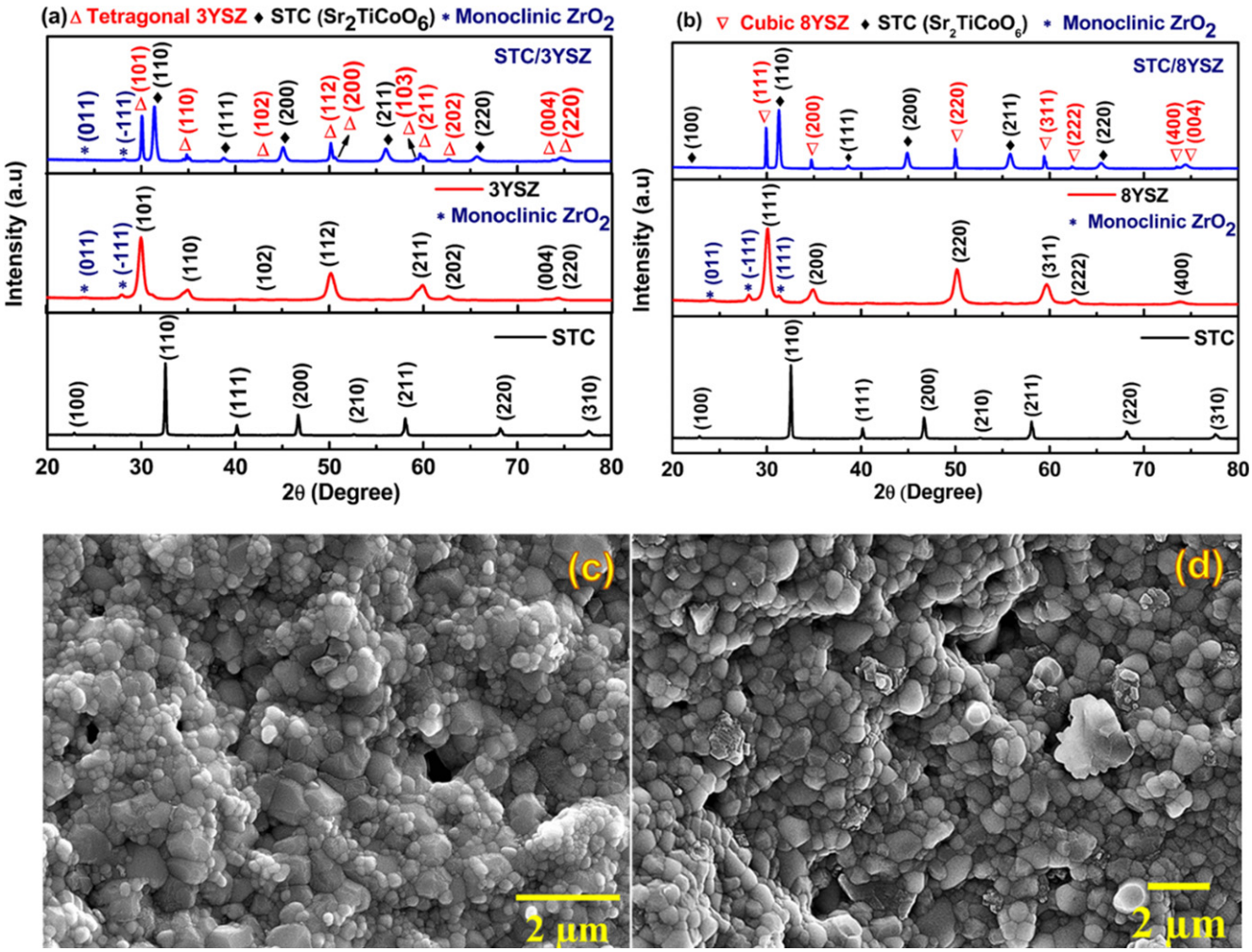

Figure 1. XRD pattern of (a) STC/3YSZ and (b) STC/8YSZ composites compared with that of STC and YSZ ceramics, and FESEM image of, (c) STC/3YSZ, and (d) STC/8YSZ composite.

curve with the Arrhenius equation as expressed below:

$$\sigma = \sigma_0 \exp\left(-\frac{E_a}{K_B T}\right), \tag{6}$$

where σ is the conductivity, σ_0 is a pre-exponential function, E_a is the activation energy, K_B is Boltzmann constant, and T is the absolute temperature. Figures 3(a) and (b) show the Arrhenius plot of grain and grain boundary polarization for STC/3YSZ and STC/8YSZ composites, respectively. The estimated activation energy for grain and grain boundary is estimated as 0.42–0.48 eV and 0.50–0.55 eV, respectively, for STC/YSZ ceramics. The obtained total activation energy for STC/3YSZ and STC/8YSZ is 0.50 and 0.52 eV, respectively, shown in figure S2. Similar values of activation energy have been observed for both the composites STC/3YSZ and STC/8YSZ, implying the occurrence of identical charge carriers.

Figures 4 and S3 depict the spectroscopic plot of frequency-dependent imaginary part of electric modulus and impedance in the temperature range from 250 °C to 650 °C for STC/8YSZ and STC/3YSZ composites, respectively. The electric modulus (M'') vs log(frequency) plot gives the well-resolved peak for grain contribution showing the existing capacitance in the grain interior. Another spectroscopic plot between Z'' vs log(frequency) illustrates the resistive process in the ceramics. The grain boundaries are found to be more resistive and capacitive compared to grain for all measured temperatures. In the ideal Debye model, the imaginary part of the electrical modulus (M'') and impedance (Z'') peak should be symmetric [44]. In STC/8YSZ, at low-temperature modulus spectra show nearly symmetric peak, but with increasing temperature, it has become asymmetric and is shifted toward the higher frequency range. Such kind of asymmetric modulus peak is attributed to the thermal relaxation process in the literature [45, 46]. Hence it can be summarized that conductivity in both composite systems is driven by thermal relaxation.

Further, we have calculated the difference between the relaxation frequencies of grain and grain boundary polarizations, and the difference is found to be higher than two orders of magnitude. The relaxation frequency of grain and grain boundary contribution is estimated from the maximum peak values of the spectroscopic plot of electric modulus (M'') and impedance (Z''). The relaxation frequency (f_r) is calculated

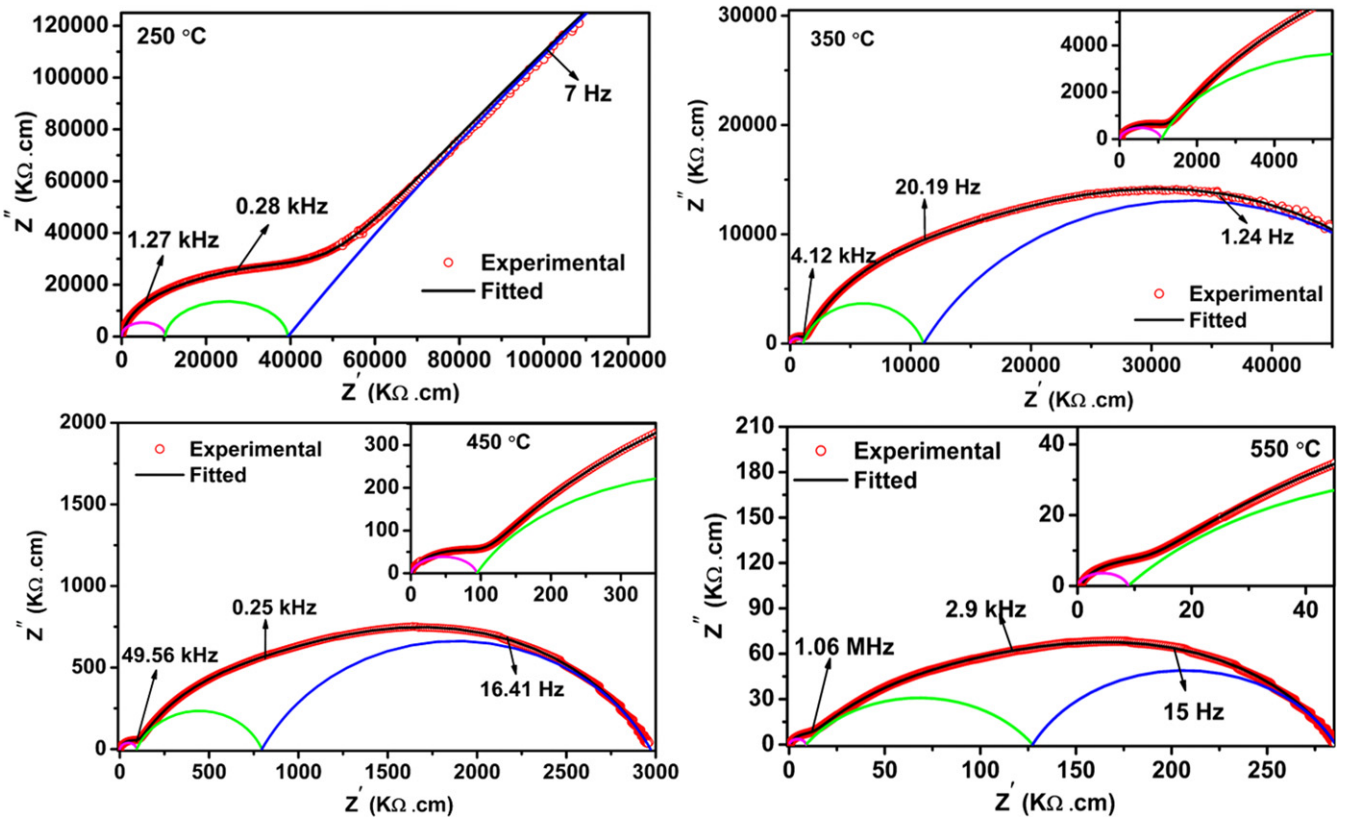

Figure 2. Complex impedance spectra of STC/8YSZ composites, Nyquist plot is fitted with R–CPE circuit (semicircles) for grain, grain boundary, and electrode contribution at various temperatures.

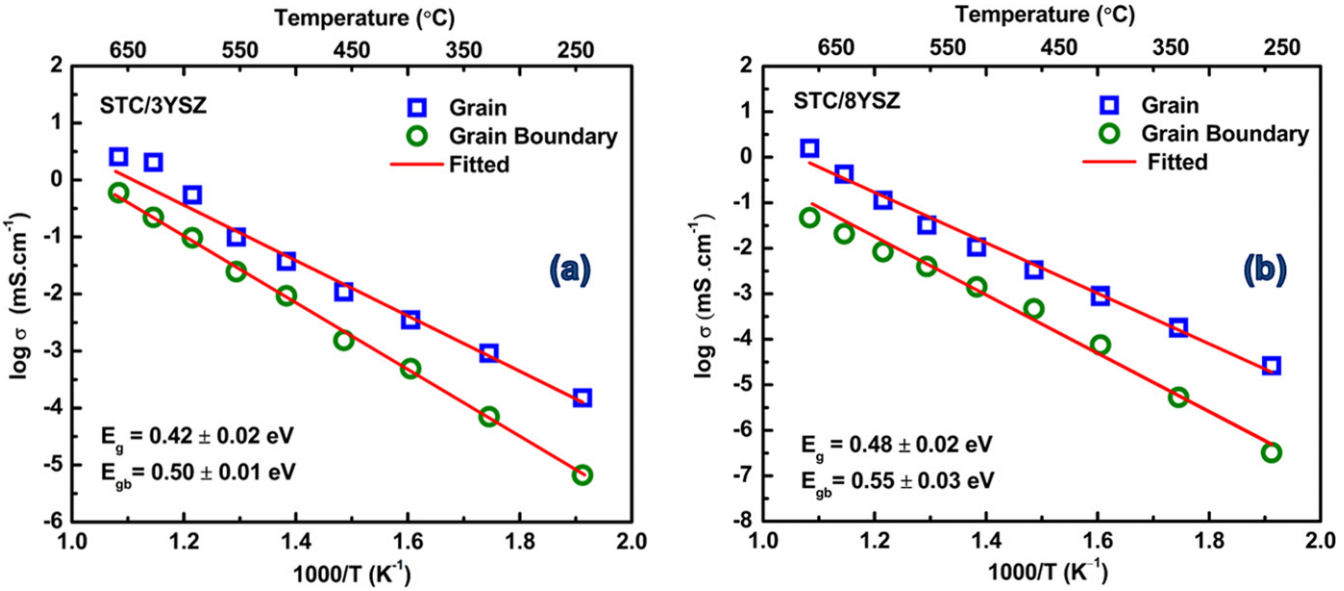

Figure 3. Arrhenius plot of conductivity vs 1000/T (a) STC/3YSZ and (b) STC/8YSZ composites.

using the following expression:

$$f_{\mathrm{r}} = \frac{1}{2\pi(RQ)^{1/n}}, \tag{7}$$

where R is resistance, and Q is the constant phase element for the circuit fitting.

Since the charge transport in this system is thermally activated, the relaxation frequency parameter usually follows Arrhenius law given by the following equation

$$f_{\mathrm{r}} = f_0 \exp\left(-\frac{E_{\mathrm{a}}}{k_{\mathrm{B}}T}\right), \tag{8}$$

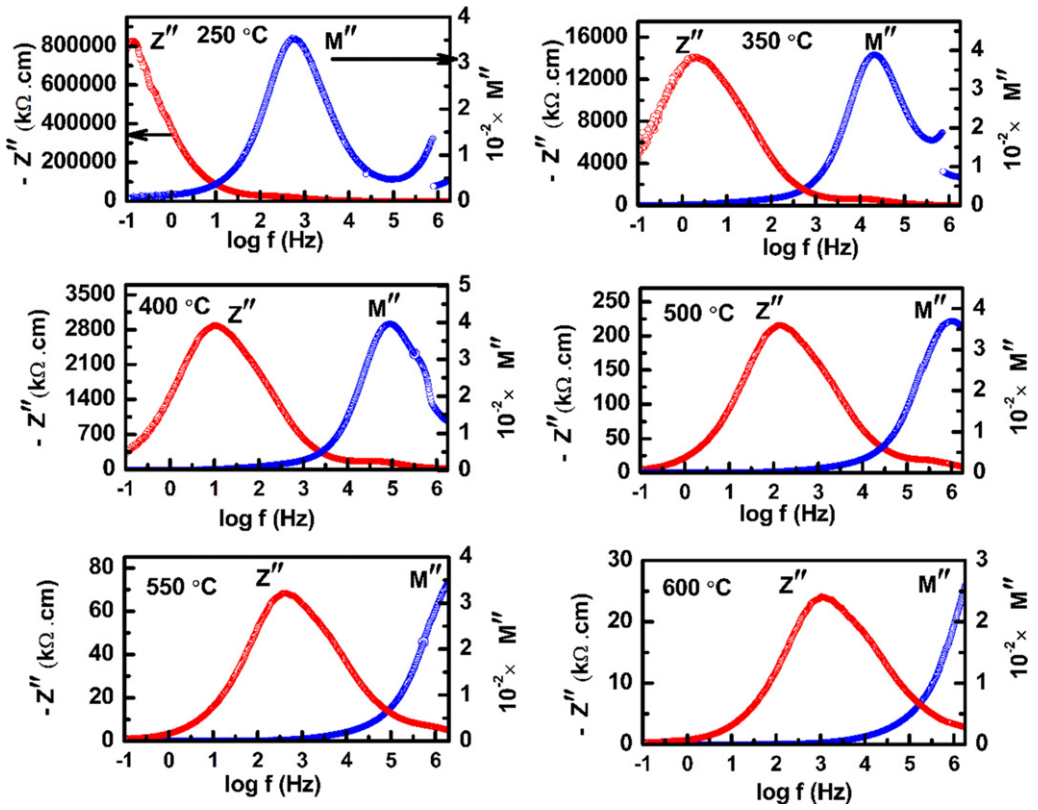

Figure 4. Frequency-dependent spectroscopic plot of Z'' and M'' for STC/8YSZ composite in the temperature range from 250 °C to 600 °C.

where f_r is the relaxation frequency, f_0 is a pre-exponential function, E_a is the activation energy, k_B is Boltzmann constant, and T is the absolute temperature. Figure 5 illustrates the variation in relaxation frequency of grain and grain boundary polarization of STC/YSZ composite material with temperature. STC/3YSZ and STC/8YSZ, both the composites exhibit higher grain boundary resistance than grain polarization resistance. STC/3YSZ shows better conductivity than STC/8YSZ, as shown in table 1. STC/8YSZ exhibits lower ionic conductivity, almost one order of magnitude low σ_{gb} than the STC/3YSZ. Activation energy calculated from the Arrhenius plot of relaxation frequency is found to be lower for STC/3YSZ composite compared to that of STC/8YSZ, suggesting easy charge carrier mobility in STC/3YSZ composites, which further corroborates well with increased conductivity values obtained in this composition. Considerable differences between the activation energy of conductivity and relaxation frequency are noticeable. According to Austin and Mott [47], this difference implies the relaxation frequency dominated by the hopping energy of charge carriers. At the same time, the overall conduction is affected by the hopping energy, disorder, and binding energy of polarons. Therefore, further discussion is required to understand the conduction and relaxation mechanism in these composites.

4. Discussion

The conduction mechanism of STC/YSZ composites in terms of ionic conductivity, AC conductivity, DC conductivity, and dielectric relaxation is analyzed using complex impedance spectroscopy data. A real part of frequency-dependent conductivity (σ') obtained from the impedance spectroscopy at different temperatures (250 °C–650 °C) is shown in figures 6(a) and S4 for STC/8YSZ and STC/3YSZ composites, respectively. Further, to elucidate the ion transport and charge carrier dynamics, the transport phenomenon is explained with the help of UDR [32]. In ceramics, two types of insulating barriers exist, such as (i) grain boundaries and (ii) domain boundaries, which restrict the motion of the charge carrier [48, 49]. In our case, grain boundaries are like insulating barriers. Moreover, the frequency-dependent charge carrier movement influences the conductivity in three ways, which are (i) long-range diffusion of charge carrier, (ii) localized carrier motion into the grains boundaries, and (iii) localized carrier motion into the domain boundaries [48]. The potential energy barrier appears as uncertainties or anomalies in the system, which is investigated using the relaxation process.

The frequency-dependent conductivity curve can be explained in three parts, low, intermediate, and high frequency region. At low frequency, conductivity is independent of frequency, which is corresponding to dc conductivity. In mid frequencies, conductivity increases nonlinearly with frequency and is seen as a dispersive region in the conductivity curve. At higher frequencies, conductivity increases linearly with frequency. Such kind of conductivity behavior can be described by Jonscher power law over a wide frequency range. Jonscher power law or UDR of conductivity can be expressed as [50]

$$\sigma'(\omega) = \sigma_{DC} + A\omega^n, \tag{9}$$

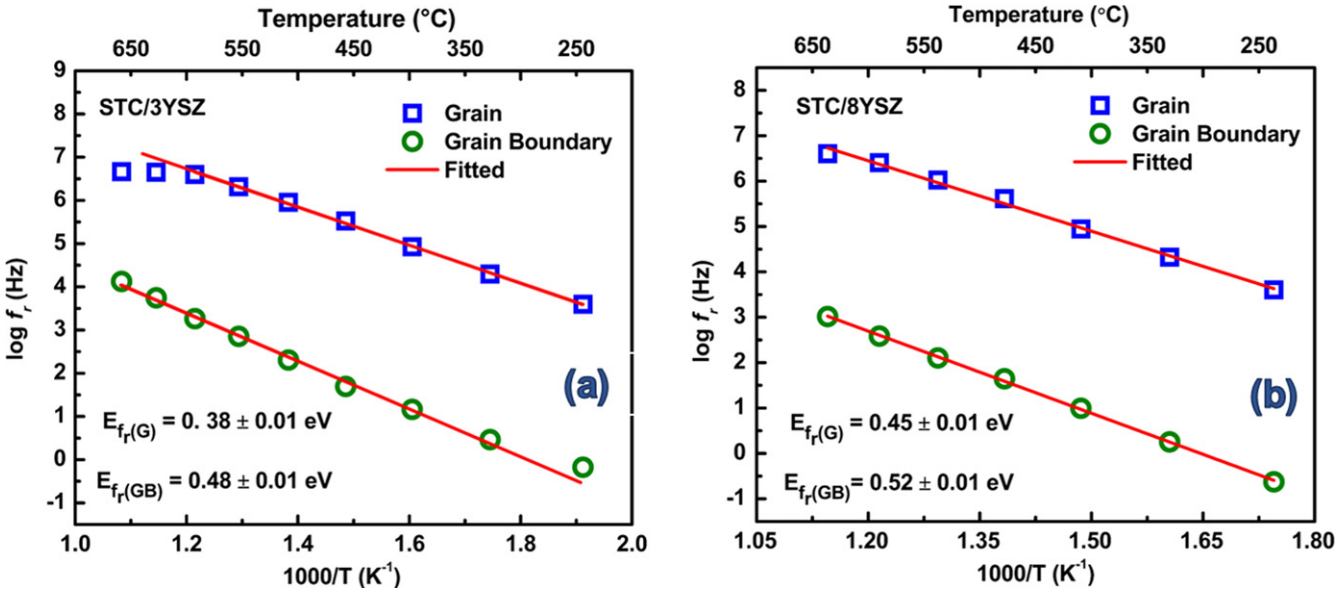

Figure 5. Arrhenius plot for relaxation frequency (f_r) vs 1000/T for grain and grain boundary polarization of (a) STC/3YSZ and (b) STC/8YSZ composite materials.

Table 1. Conductivity for grain (σ_g), grain boundary (σ_{gb}), and total (σ_{Total}) obtained from Nyquist plot fitting at temperature 650 °C, activation energy for grain and grain boundary is calculated from the fitting data and relaxation frequency of modulus spectra for STC/YSZ composites[a].

Composites	Conductivity (from Nyquist fitting)			Activation energy			
				Using Nyquist fitting		Using modulus spectroscopy	
	σ_g (mS cm^{-1})	σ_{gb} (mS cm^{-1})	σ_{Total} (mS cm^{-1})	E_g (eV)	E_{gb} (eV)	E_g (eV)	E_{gb} (eV)
STC/3YSZ	2.55	0.59	0.49	0.42	0.50	0.38	0.48
STC/8YSZ	1.58	0.06	0.05	0.48	0.55	0.45	0.52

[a]σ_g = grain conductivity; σ_{gb} = grain boundary conductivity; σ_{Total} = total conductivity (from Nyquist fitting)

where A is a constant, σ_{DC} is DC conductivity, and n is an exponent. If n lies between $0.5 < n < 0.7$, i.e., complex conductivity obeys UDR behavior [51].

Conductivity is strongly dependent on frequency in the intermediate region. AW [52, 53], found that the Jonscher power law is not valid over the entire range of frequencies as $\omega \to 0$ and subsequently proposed the hopping frequency (ω_C) of carriers. Therefore the modified Jonscher law known as AW power law can be expressed by the following formula [54]

$$\sigma' = \sigma_{DC}\left[1 + \left(\frac{\omega}{\omega_C}\right)^n\right], \tag{10}$$

where σ_{DC} is DC conductivity, ω_C is the crossover or hopping frequency of ionic carriers, and n is an exponent lies between ($0 \leqslant n \leqslant 1$).

Figure 6(a) shows the non-negligible electrode polarization at low frequency in the low temperatures. This electrode polarization is decreased with increasing temperature, and DC contribution appears clearly while at 250 °C, $\sigma'(\omega)$ drops sharply below the limiting value of DC conductivity infers the frequency crossover [55]. Figures 6(a) and S4(a) demonstrates the frequency-dependent conductivity curve, which is fitted using the AW power law for STC/8YSZ and STC/3YSZ, respectively. DC conductivity (σ_{DC}), crossover frequency (ω_C), and exponent (n) obtained from the AW fitting, are presented in table 2 for STC/8YSZ and STC/3YSZ composites. The exponent (n) is found to be decreased with increasing temperature. The values of exponent (n) attained from the AW power law lie in the range of Jonscher regime of UDR for STC/8YSZ and STC/3YSZ ionic solids. In σ' vs frequency plot, a plateau region appears at low frequency, which is shifted toward the higher frequency with increasing temperature. This frequency-independent conductivity assigned as DC conductivity (σ_{DC}) or long-range ionic conductivity is found to be increased monotonically with temperature, as shown in table 2. At high temperatures, the characteristic plateau region corresponding to DC conductivity becomes more prominent, suggesting ease of transport of charge carriers, which encounter thermal activation energy barrier due to localization, especially in the grain boundaries.

Almost four decades ago, Barton [56], Nakajima [57], and Namikawa [58] (BNN) gave an empirical relation which correlates between the electrical conductivity and dielectric strength. BNN relation defines the crossover frequency ($\omega_c = 1/\tau_C$) from DC conductivity to the dispersive region

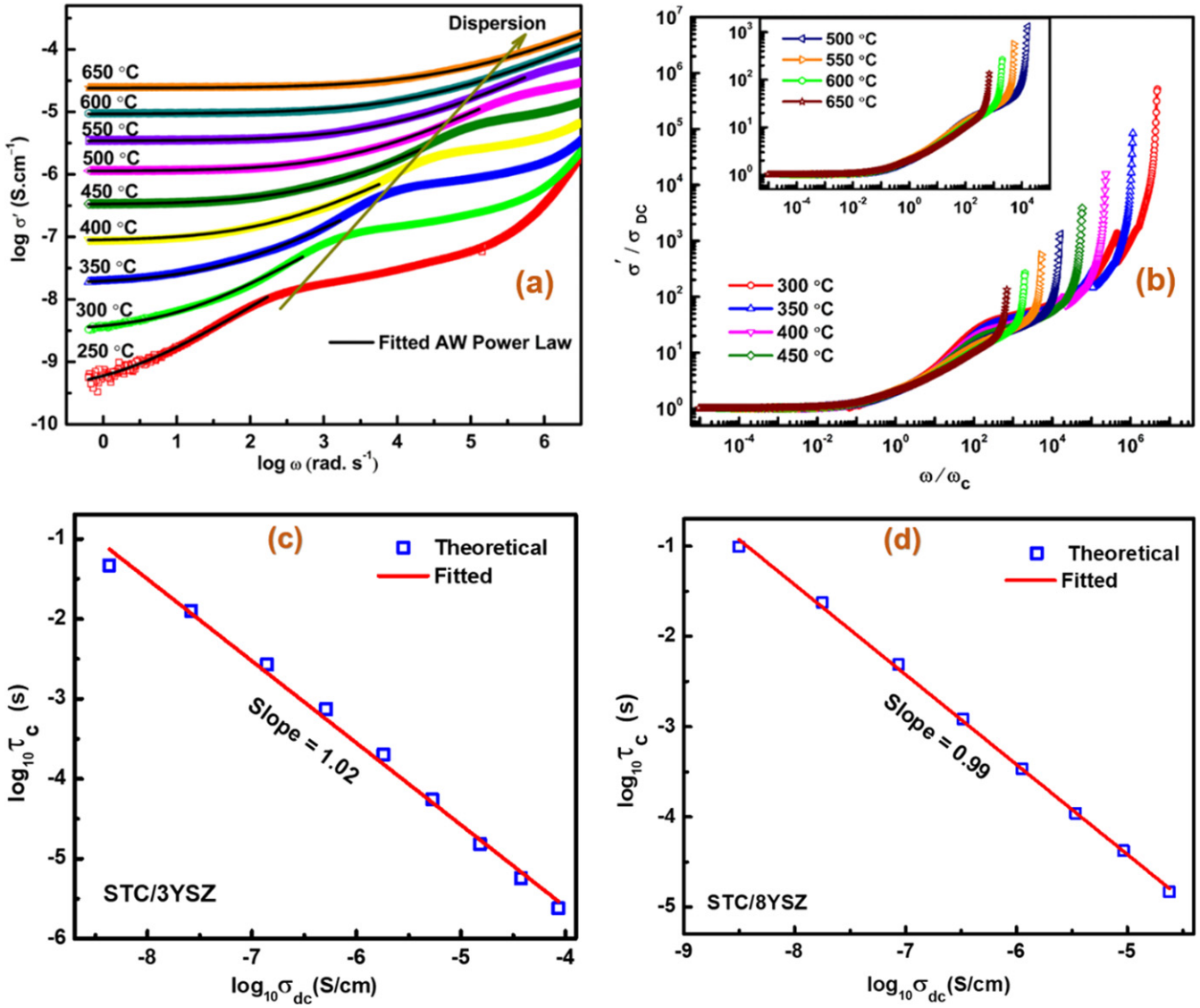

Figure 6. (a) Frequency-dependent AC conductivity fitted using AW power law, (b) scaling of ac conductivity according to TTSP for STC/8YSZ composite at different temperatures from 250 °C–650 °C, and plot of $\log_{10}\sigma_{DC}$ vs $\log_{10}\tau_C$, showing the BNN relation for (c) STC/3YSZ and (d) STC/8YSZ composites.

which can be expressed as follows [59, 60]

$$\sigma_{DC} = \frac{p\varepsilon_0\Delta\varepsilon}{\tau_C}, \tag{11}$$

where p is a numerical constant of order 1, ε_0 is the permittivity of free space, $\Delta\varepsilon$ is dielectric strength and τ_C is relaxation time calculated from the crossover frequency. Figures 6(c) and (d) display the log–log plot between DC conductivity and the relaxation time for these composites based on the data attained from equation (10). Graph figures 6(c) and (d) illustrates the linear relationship (slop ∼1 or close to unity) between DC conductivity and relaxation time, which infers the presence of single transport mechanisms and interrelated AC and DC conduction.

With increasing temperature, the manifold increase in crossover frequency (ω_C) is found, separating DC and AC conductivity, as illustrated in table 2. As a consequence, the conductivity dispersion region moves toward the higher frequencies with increasing temperature suggesting conductivity scaling. Conductivity scaling can be expressed by TTSP, which is stated by the following expression [39, 61]

$$\frac{\sigma'}{\sigma_{DC}} = f_s\left(\frac{\omega}{\omega_c}\right), \tag{12}$$

where f_s is the scaling function which is independent of temperature and described the ion dynamics in the system, σ' is a real part of complex conductivity, σ_{DC} is DC conductivity, and ω_c is the crossover frequency. Figures 6(b) and S4(b) demonstrate the conductivity scaling curve for STC/8YSZ and STC/3YSZ composites, respectively. Here σ_{DC} and ω_c are physical parameters and form a master curve for conductivity with increasing temperature. In the low frequency region, the conductivity scaling curve lies on the single master curve and subsequently obeys TTSP [62] but not in the entire frequency regime. However, TTSP is followed in a broader frequency

Table 2. DC conductivity (σ_{DC}), crossover frequency or hopping frequency (ω_C), and exponent (n) obtained from AW power law fitting of ac conductivity with frequency plot for STC/8YSZ and STC/3YSZ composites respectively, from temperature 250 °C–650 °C.

Composites	STC/8YSZ			STC/3YSZ		
Temperature (°C)	DC conductivity (σ_{DC}/S × cm^{-1})	Crossover frequency (ω_C/rad s^{-1})	Exponent (n)	DC conductivity (σ_{DC}/S × cm^{-1})	Crossover frequency (ω_C/rad s^{-1})	Exponent (n)
250	1.05×10^{-10}	1	0.72	4.30×10^{-9}	21	0.65
300	3.14×10^{-9}	10	0.67	2.62×10^{-8}	79	0.57
350	1.78×10^{-8}	42	0.60	1.39×10^{-7}	371	0.52
400	8.64×10^{-8}	206	0.59	5.13×10^{-7}	1340	0.49
450	3.29×10^{-7}	825	0.58	1.81×10^{-6}	4983	0.44
500	1.12×10^{-6}	2960	0.57	5.33×10^{-6}	18 247	0.43
550	3.42×10^{-6}	9192	0.55	1.53×10^{-5}	66 079	0.42
600	9.24×10^{-6}	23 869	0.50	3.77×10^{-5}	176 036	0.41
650	2.39×10^{-5}	67 671	0.49	8.59×10^{-5}	468 043	0.41

range in the higher temperatures, especially above 500 °C, as shown in the inset of figures 6(b) and S4(b).

The permittivity spectra have been studied further to understand the other anomalies in the STC/YSZ composites. Figures 7(a), (b) and S5(a), (b) display the frequency-dependent real (ε') and imaginary (ε'') part of permittivity estimated from impedance data at various temperatures for STC/8YSZ and STC/3YSZ composites, respectively. In general, real (ε') and imaginary (ε'') part of complex permittivity increases monotonically with increasing temperature, but with increasing frequency, permittivity starts decreasing in inhomogeneous systems. Similar behavior has been reported [63–65] in the literature. Koop's theory [49] can explain this frequency-dependent behavior of permittivity in composite, inhomogeneous systems, etc. According to this model, the inhomogeneous system consists of conducting grains separated by the poorly performing grain boundaries such that ions start to pile up at the grain boundaries. Therefore, grain boundaries become more resistive and capacitive and give rise to polarization [49]. Consequently, the polarization resistance of grain boundaries becomes much higher than the grain polarization resistance. Therefore, grain conductivity is larger than the conductivity of grain boundaries, and these grain boundaries are acting here as an insulating barrier. The step-like decrease is observed in both ε' and ε'' spectra due to molecular reorientation. At low frequencies, dielectric permittivity (ε') and dielectric loss (ε'') is increased manifold with increasing temperature for both STC/YSZ composites, as shown in figures 7(a), (b), and S6(a), (b), respectively. This increment in permittivity implies the existence of interfacial polarization in the ionic conductors [66, 67]. The occurrence of larger imaginary permittivity is possibly due to space charge accumulation at the grain boundary, which suggests the high ohmic losses at the interfaces of the materials. These ohmic losses occur due to resistance between the electrode and bulk, which causes performance degradation of the devices. ε' and ε'' decrease sharply as moving toward the higher frequencies, which suggests the reduction in interfacial polarization. Therefore, conductivity enhances with temperature. At low temperatures, relaxation occurs due to the localized motion of carriers, but at high temperature, hopping behavior starts dominating. Further, to comprehend the presence of the relaxation process in the inhomogeneous composite system, the DC conduction free dielectric loss (ε''_{der}) was calculated using the following expression [68–70]

$$\varepsilon''_{der} = -\frac{\pi}{2} \times \frac{\partial \varepsilon'(f)}{\partial(\ln f)} \tag{13}$$

$\varepsilon'(\omega)$ is the real part of complex permittivity, and f is the frequency. Figure 7(c) and S5(c) illustrate the graph of DC conduction free loss (ε''_{der}) with frequency. The derivative loss spectra show the step in the same position as shown in the ε' spectra, which suggests the transition of carriers [68]. Two types of relaxation process are visible in dielectric loss (ε''_{der}) spectra shown in figures 7(c) and S5(c). At low frequency, interfacial polarization phenomenon occurs while at high frequency, the relaxation arises owing to the confined motion of carriers into the potential well [70]. Hypothetically, such transition occurs due to the Maxwell Wagner Sillars process in which ions are accumulated at the interfaces or grain boundaries of the phase-separated materials. Interfacial polarization also exists between the contact electrode and materials.

Additionally, Kramers Kronig transformation validates the impedance spectroscopy data by applying the linearity condition [71, 72]. ε' and ε'' are interrelated by Kramers Kronig transformation [73]. In this approach, ε' is proportional to the power law of ac conductivity (f^m) and satisfying $\varepsilon' = Bf^{m-1}$, which can be expressed as [74]

$$\varepsilon' f = Bf^m, \tag{14}$$

where f is the frequency, B is constant, and m is the exponent and obtained from the slope of the graph between $\log(\varepsilon' f)$ vs $\log(f)$. It can be seen from figures 7(d) and S5(d) that the $\varepsilon' f$ becomes nearly linear at low temperatures and high frequency region. With increasing temperature, this linear region is shifted toward the high frequency range due to the relaxation process. At 250 °C, the value of exponent m observed from the fitting is ∼1.0 for both STC/YSZ composites, as shown in the inset of figures 7(d) and S5(d). The value of m close to unity indicates the presence of other anomaly. Nevertheless, with increasing temperature, m starts decreasing, which implies that UDR starts dominating the

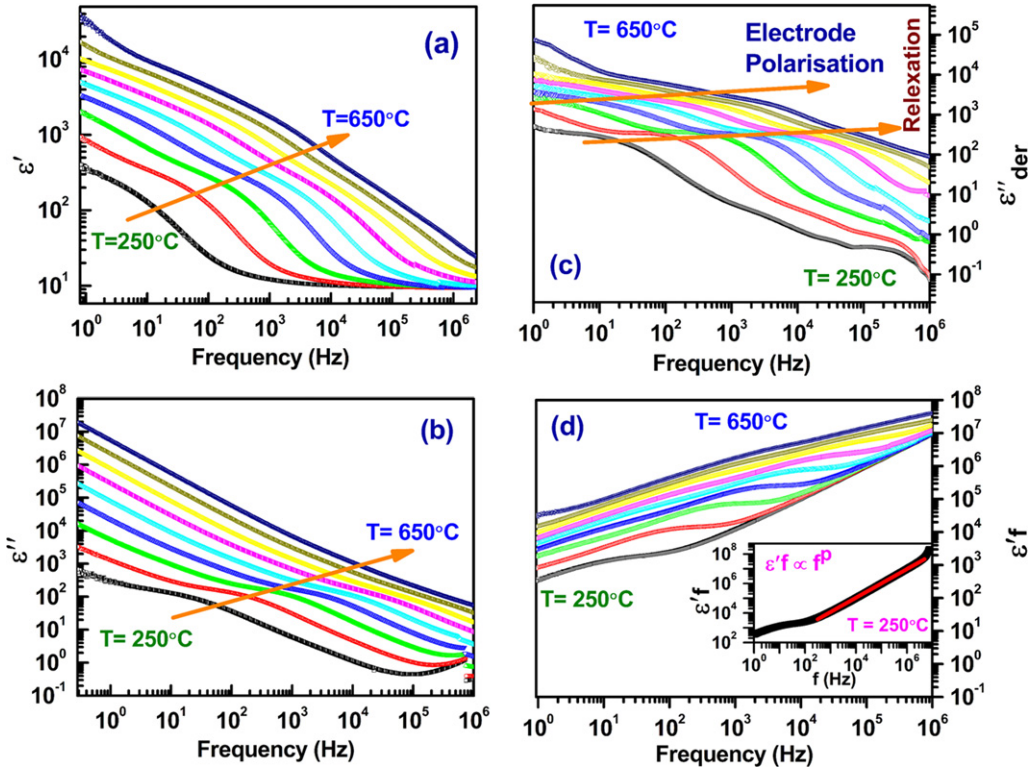

Figure 7. Frequency-dependent permittivity plot in the temperature range from 250 °C to 650 °C for STC/8YSZ composite, (a) real part of permittivity (ε') (b) imaginary part of permittivity (ε''), (c) DC conduction free dielectric loss (ε''_{der}), (d) Plot of $\varepsilon' f$ as a function of frequency and inset of (d) showing the Kramers Kronig transformation curve at 250 °C.

transport. These anomalies effectively describe the polarization, charge carrier hopping, electronic, ionic, or polaronic nature in inhomogeneous, disordered solids.

5. Conclusions

In summary, we have determined the conduction mechanism in STC/YSZ composites through impedance spectroscopy, modulus, and dielectric spectra. The grain, grain boundary conductivity for composites have been calculated using the Nyquist fitting and found to be increased with temperature. The total conductivity obtained from the Nyquist fitting is 0.49 S cm^{-1} and 0.05 S cm^{-1} at 650 °C for STC/3YSZ and STC/8YSZ composites, respectively, which can be used as electrode materials in the solid oxide fuel cell. Conductivity from Nyquist fitting and relaxation frequency from modulus obey the Arrhenius behavior. Further, UDR model explains the conduction mechanism of charge carriers. AC conductivity of STC/YSZ composites follow the AW power law. The exponent (n) value obtained from AW power law fitting lies in the range 0.7–0.4 for STC/YSZ, which validated the Jonscher regime and ions hopping occurs in the composites systems. The conductivity scaling obeys TTSP, where AC conductivity curve lies onto one master curve in an explicit frequency range. AC and DC conduction are interrelated to each other. DC conduction free dielectric loss has explained the dielectric relaxation due to the localized motion of charge carriers at low frequency. The inhomogeneous system consists of conductive grains, separated by the poorly performing grain boundaries, and interfacial polarization ensues between the material and electrode. Furthermore, Kramers Kronig transformation validates the impedance spectra data. The Kramers Kronig exponent shows lower m values in the UDR region. Therefore, UDR is found to be powerful tool to study the charge transport mechanism in STC/YSZ, which can be further used for other composites and disordered solids.

Author contributions

SS synthesized the samples and conducted the experiments. SS analyzed the data and wrote the manuscript with the help of TM. KB helped editing the manuscript. TM was responsible for the original research concept, designing the philosophy of experiments and physical interpretation.

Acknowledgments

This work is supported by the grant from Science and Engineering Research Board, DST (SERB-DST), India (Grant No. IMP/2018/000955).

Data availability statement

All data that support the findings of this study are included within the article (and any supplementary files).

ORCID iDs

Sudha Saini https://orcid.org/0000-0001-5853-5479
Kantesh Balani https://orcid.org/0000-0003-0619-9164
Tanmoy Maiti https://orcid.org/0000-0003-1581-7614

References

[1] Luo H, Efimov K, Jiang H, Feldhoff A, Wang H and Caro J 2011 CO_2-stable and cobalt-free dual-phase membrane for oxygen separation *Angew. Chem., Int. Ed.* **50** 759–63
[2] Ding D, Li X, Lai S Y, Gerdes K and Liu M 2014 Enhancing SOFC cathode performance by surface modification through infiltration *Energy Environ. Sci.* **7** 552–75
[3] Miao F, Yi W, Goldfarb I, Yang J J, Zhang M-X, Pickett M D, Strachan J P, Medeiros-Ribeiro G and Williams R S 2012 Continuous electrical tuning of the chemical composition of TaOx-based memristors *ACS Nano* **6** 2312–8
[4] Aoki Y, Wiemann C, Feyer V, Kim H-S, Schneider C M, Ill-Yoo H and Martin M 2014 Bulk mixed ion electron conduction in amorphous gallium oxide causes memristive behaviour *Nat. Commun.* **5** 1–9
[5] Tarascon J M, Delacourt C, Prakash A S, Morcrette M, Hegde M S, Wurm C and Masquelier C 2004 Various strategies to tune the ionic/electronic properties of electrode materials *Dalton Trans.* **19** 2988–94
[6] Lin Y, Fang S, Su D, Brinkman K S and Chen F 2015 Enhancing grain boundary ionic conductivity in mixed ionic–electronic conductors *Nat. Commun.* **6** 6824
[7] Wang H, Werth S, Schiestel T and Caro J 2005 Perovskite hollow-fiber membranes for the production of oxygen-enriched air *Angew. Chem., Int. Ed.* **44** 6906–9
[8] Wachsman E D and Lee K T 2011 Lowering the temperature of solid oxide fuel cells *Science* **334** 935–9
[9] Jacobson A J 2010 Materials for solid oxide fuel cells *Chem. Mater.* **22** 660–74
[10] Maier J 2005 Nanoionics: ion transport and electrochemical storage in confined systems *Nat. Mater.* **4** 805–15
[11] Carollo G, Garbujo A, Mauvy F and Glisenti A 2020 Critical raw material-free catalysts and electrocatalysts: complementary strategies to activate economic, robust, and ecofriendly $SrTiO_3$ *Energy Fuels* **34** 11438–48
[12] Blennow P, Hansen K K, Wallenberg L R and Mogensen M 2008 Strontium titanate-based composite anodes for solid oxide fuel cells *Ecs Trans.* **13** 181
[13] Fu Q, Tietz F, Sebold D, Tao S and Irvine J T S 2007 An efficient ceramic-based anode for solid oxide fuel cells *J. Power Sources* **171** 663–9
[14] Fagg D P, Kharton V V, Kovalevsky A V, Viskup A P, Naumovich E N and Frade J R 2001 The stability and mixed conductivity in La and Fe doped $SrTiO_3$ in the search for potential SOFC anode materials *J. Eur. Ceram. Soc.* **21** 1831–5
[15] Verbraeken M C, Ramos T, Agersted K, Ma Q, Savaniu C D, Sudireddy B R, Irvine J T S, Holtappels P and Tietz F 2015 Modified strontium titanates: from defect chemistry to SOFC anodes *RSC Adv.* **5** 1168–80
[16] Yang Q Q, Meng B, Lin Z L, Zhu X K, Yang F and Wu S 2017 Effect of sintering temperature on the elemental diffusion and electrical conductivity of $SrTiO_3$/YSZ composite ceramic *Ionics* **23** 967–75
[17] Dayaghi A M, Kim K J, Kim S, Park J, Kim S J, Park B H and Choi G M 2016 Stainless steel-supported solid oxide fuel cell with $La_{0.2}Sr_{0.8}Ti_{0.9}Ni_{0.1}O_{3-\delta}$/yttria-stabilized zirconia composite anode *J. Power Sources* **324** 288–93
[18] Cho S, Fowler D E, Miller E C, Cronin J S, Poeppelmeier K R and Barnett S A 2013 Fe-substituted $SrTiO_{3-\delta}$–$Ce_{0.9}Gd_{0.1}O_2$ composite anodes for solid oxide fuel cells *Energy Environ. Sci.* **6** 1850–7
[19] Muhoza S P, Barrett T E, Soll S E and Gross M D 2017 Nanostructured SOFC electrode scaffolds prepared via high temperature *in situ* carbon templating of hybrid materials *ECS Trans.* **78** 1407
[20] Masó N and West A R 2015 Electronic conductivity in yttria-stabilized zirconia under a small dc bias *Chem. Mater.* **27** 1552–8
[21] Garcia-Barriocanal J, Rivera-Calzada A, Varela M, Sefrioui Z, Iborra E, Leon C, Pennycook S J and Santamaria J 2008 *Science* **321** 676–80
[22] Ma Q, Tietz F, Sebold D and Stöver D 2010 *J. Power Sources* **195** 1920–5
[23] Kolodiazhnyi T and Petric A 2005 The applicability of Sr-deficient n-type $SrTiO_3$ for SOFC anodes *J. Electroceram.* **15** 5–11
[24] Hussain A M, Høgh J V, Jacobsen T and Bonanos N 2012 Nickel–ceria infiltrated Nb-doped $SrTiO_3$ for low temperature SOFC anodes and analysis on gas diffusion impedance *Int. J. Hydrog. Energy* **37** 4309–18
[25] Bochentyn B, Karczewski J, Gazda M, Jasiński P and Kusz B 2013 Interactions between components of $SrTi_{0.98}Nb_{0.02}O_{3-\delta}$–YSZ and $SrTi_{0.98}Nb_{0.02}O_{3-\delta}$–$CeO_2$ composites *Phys. Status Solidi a* **210** 538–45
[26] He H, Huang Y, Vohs J M and Gorte R J 2004 Characterization of YSZ–YST composites for SOFC anodes *Solid State Ion.* **175** 171–6
[27] Huang Y, Vohs J M and Gorte R J 2005 Characterization of LSM–YSZ composites prepared by impregnation methods *J. Electrochem. Soc.* **152** A1347
[28] Saxena M, Balani K and Maiti T 2019 Structure and thermoelectric properties of calcium doped Sr_2TiCoO_6 double perovskites *Mater. Sci. Eng.* B **244** 65–71
[29] Bakkali H, Dominguez M, Batlle X and Labarta A 2016 Universality of the electrical transport in granular metals *Sci. Rep.* **6** 29676
[30] Jonscher A K 1977 The 'universal' dielectric response *Nature* **267** 673–9
[31] Jonscher A K 1975 A new model of dielectric loss in polymers *Colloid Polym. Sci.* **253** 231–50
[32] Jonscher A K 1999 Dielectric relaxation in solids *J. Phys. D: Appl. Phys.* **32** R57
[33] Dyre J C and Schrøder T B 2000 Universality of ac conduction in disordered solids *Rev. Mod. Phys.* **72** 873
[34] Almond D P and Vainas B 1999 The dielectric properties of random R–C networks as an explanation of the 'universal' power law dielectric response of solids *J. Phys.: Condens. Matter.* **11** 9081
[35] Almond D P and Bowen C 2004 Anomalous power law dispersions in ac conductivity and permittivity shown to be characteristics of microstructural electrical networks *Phys. Rev. Lett.* **92** 157601
[36] Bouamrane R and Almond D P 2003 The emergent scaling phenomenon and the dielectric properties of random resistor-capacitor networks *J. Phys.: Condens. Matter.* **15** 4089
[37] Vainas B, Almond D P, Luo J and Stevens R 1999 An evaluation of random R–C networks for modelling the bulk ac electrical response of ionic conductors *Solid State Ion.* **126** 65–80
[38] Almond D P, Bowen C R and Rees D A S 2006 *J. Phys. D: Appl. Phys.* **39** 1295
[39] Sidebottom D L 1999 Universal approach for scaling the ac conductivity in ionic glasses *Phys. Rev. Lett.* **82** 3653
[40] Steeman P A M and Van Turnhout J 1997 A numerical Kramers–Kronig transform for the calculation of dielectric relaxation losses free from Ohmic conduction losses *Colloid Polym. Sci.* **275** 106–15

[41] Johnson D 1990 Zview *(Version 3.1 C) Scribner Associates Inc Southern Pines, North Carolina*

[42] Vendrell X and West A R 2018 Electrical properties of yttria-stabilized zirconia, YSZ single crystal: local AC and long range DC conduction *J. Electrochem. Soc.* **165** F966–75

[43] Grant F A 1958 Use of complex conductivity in the representation of dielectric phenomena *J. Appl. Phys.* **29** 76–80

[44] Liu J, Duan C-G, Yin W-G, Mei W-N, Smith R W and Hardy J R 2004 Large dielectric constant and Maxwell–Wagner relaxation in $Bi_{2/3}Cu_3Ti_4O_{12}$ *Phys. Rev.* B **70** 144106

[45] Hodge I M, Ingram M D and West A R 1976 Impedance and modulus spectroscopy of polycrystalline solid electrolytes *J. Electroanal. Chem. Interfacial Electrochem.* **74** 125–43

[46] Singh D N, Sinha T P and Mahato D K 2017 Electric modulus, scaling and ac conductivity of La_2CuMnO_6 double perovskite *J. Alloys Compd.* **729** 1226–33

[47] Austin I G and Mott N F 1969 Polarons in crystalline and non-crystalline materials *Adv. Phys.* **18** 41–102

[48] Li W and Schwartz R W 2006 Ac conductivity relaxation processes in $CaCu_3Ti_4O_{12}$ ceramics: grain boundary and domain boundary effects *Appl. Phys. Lett.* **89** 242906

[49] Koops C G 1951 On the dispersion of resistivity and dielectric constant of some semiconductors at audiofrequencies *Phys. Rev.* **83** 121

[50] Jonscher A K 1978 Low-frequency dispersion in carrier-dominated dielectric *Phil. Mag.* B **38** 587–601

[51] Nowick A S, Vaysleyb A V and Kuskovsky I 1998 Universal dielectric response of variously doped CeO_2 ionically conducting ceramics *Phys. Rev.* B **58** 8398

[52] Nowick A S, Lim B S and Vaysleyb A V 1994 Nature of the ac conductivity of ionically conducting crystals and glasses *J. Non-Cryst. Solids* **172–174** 1243–51

[53] Nowick A S and Lim B S 1994 Analysis of ac conductivity data for $Na_2O_3SiO_2$ glass by stretched exponential and Jonscher power-law methods *J. Non-Cryst. Solids* **172–174** 1389–94

[54] Jonscher A 1996 The transformation program involves an extrapolation of the data by one decade on either side of the experimental frequency range *Dielectric Relaxation in Solids* (New York: Chelsea) p 54

[55] Macdonald J R 2005 *J. Phys.: Condens. Matter.* **17** 4369

[56] Barton J 1966 Dielectric relaxation of some ternary alkali–alkaline earth-silicate glasses *Verres Refract.* **20** 328–35

[57] Nakajima T 1971 Correlation between electrical conduction and dielectric polarization in inorganic glasses *Conf. on Electrical Insulation & Dielectric Phenomena-Annual Report* (Piscataway, NJ: IEEE) pp 168–76

[58] Namikawa H 1975 Characterization of the diffusion process in oxide glasses based on the correlation between electric conduction and dielectric relaxation *J. Non-Cryst. Solids* **18** 173–95

[59] Macdonald J R 2005 Universality, the Barton Nakajima Namikawa relation, and scaling for dispersive ionic materials *Phys. Rev.* B **71** 184307

[60] Tsonos C, Kanapitsas A, Kechriniotis A and Petropoulos N 2012 AC and DC conductivity correlation: the coefficient of Barton–Nakajima–Namikawa relation *J. Non-Cryst. Solids* **358** 1638–43

[61] Ghosh A and Pan A 2000 Scaling of the conductivity spectra in ionic glasses: dependence on the structure *Phys. Rev. Lett.* **84** 2188

[62] Murugavel S and Roling B 2002 AC conductivity spectra of alkali tellurite glasses: composition-dependent deviations from the Summerfield scaling *Phys. Rev. Lett.* **89** 195902

[63] Tang R, Jiang C, Qian W, Jian J, Zhang X, Wang H and Yang H 2015 Dielectric relaxation, resonance and scaling behaviors in $Sr_3Co_2Fe_{24}O_{41}$ hexaferrite *Sci. Rep.* **5** 13645

[64] Murugaraj R, Govindaraj G and George D 2002 Ac conductivity relaxation processes and its scaling behavior in sodium bismuthate glasses *J. Mater. Sci.* **37** 5101–6

[65] Bao J, Zhou J, Yue Z, Li L and Gui Z 2002 Dielectric behavior of Mn-substituted Co_2Z hexaferrites *J. Magn. Magn. Mater.* **250** 131–7

[66] Geirhos K, Lunkenheimer P, Michl M, Reuter D and Loidl A 2015 Communication: conductivity enhancement in plastic-crystalline solid-state electrolytes *J. Chem. Phys.* **143** 081101

[67] Rahmouni H, Smari M, Cherif B, Dhahri E and Khirouni K 2015 Conduction mechanism, impedance spectroscopic investigation and dielectric behavior of $La_{0.5}Ca_{0.5-x}Ag_xMnO_3$ manganites with compositions below the concentration limit of silver solubility in perovskites ($0 \leqslant x \leqslant 0.2$) *Dalton Trans.* **44** 10457–66

[68] Zhang S and Runt J 2004 Segmental dynamics and ionic conduction in poly(vinyl methyl ether)−Lithium perchlorate complexes *J. Phys. Chem* B **108** 6295–302

[69] Fragiadakis D, Dou S, Colby R H and Runt J 2008 Molecular mobility, ion mobility, and mobile ion concentration in poly(ethylene oxide)-based polyurethane ionomers *Macromolecules* **41** 5723–8

[70] Dam T, Karan N K, Thomas R, Pradhan D K and Katiyar R S 2015 Observation of ionic transport and ion-coordinated segmental motions in composite (polymer-salt-clay) solid polymer electrolyte *Ionics* **21** 401–10

[71] Boukamp B A 1995 A linear Kronig–Kramers transform test for immittance data validation *J. Electrochem. Soc.* **142** 1885–94

[72] Gabrielli C, Keddam M and Takenouti H 1993 *Electrochemical Impedance: Analysis and Interpretation* (West Conshohocken, PA: ASTM International)

[73] Lee W K, Liu J F and Nowick A S 1991 Limiting behavior of ac conductivity in ionically conducting crystals and glasses: a new universality *Phys. Rev. Lett.* **67** 1559

[74] Ke S, Huang H, Ren L and Wang Y 2009 Nearly constant dielectric loss behavior in poly (3-hydroxybutyrate-co-3-hydroxyvalerate) biodegradable polyester *J. Appl. Phys.* **105** 096103